International Journal of Biological Macromolecules 305 (2025) 140856

Contents lists available at ScienceDirect

International Journal of Biological Macromolecules

journal homepage: www.elsevier.com/locate/ijbiomac

Dual responsive phase behavior of nonionic cellulose-based polymer brushes by visible-light-driven organocatalyzed atom transfer radical polymerization

Muhammad Asif Iqbal [a], Sadaf Ul Hassan [b], Asif Mahmood [c], Waheed Al-Masry [c], Junhyuk Lee [d], Hyun Jong Lee [e], Toheed Akhter [e,*], Chan Ho Park [e,*]

[a] Department of Chemistry, School of Science, University of Management and Technology, C-II, Johar Town, 54770 Lahore, Pakistan
[b] Department of Chemistry, COMSATS University Islamabad, Lahore Campus, Lahore, Defence Road, Off Raiwind Road, Lahore 54000, Pakistan
[c] Department of Chemical Engineering, College of Engineering, King Saud University, Riyadh 11421, Saudi Arabia
[d] Korea Packaging Center, Korea Institute of Industrial Technology, Bucheon 14449, Republic of Korea
[e] Department of Chemical and Biological Engineering, Gachon University, Seongnam 13120, Republic of Korea

ARTICLE INFO

Keywords:
Hydroxypropyl cellulose
Poly(vinylpyrrolidone)
Organocatalysis
O-ATRP
Lower critical solution temperature
Dual response

ABSTRACT

Hydroxypropyl cellulose (HPC) is a nonionic, thermo-responsive polymer with temperature-dependent phase behavior. This behavior can be modified by grafting molecular units and polymer brushes onto the cellulose backbone. However, the thermo-response of such modified celluloses under biological and environmental conditions, such as pH, has been scarcely reported. This study details the synthesis and characterization of dual-temperature- and pH-responsive poly(vinyl pyrrolidone)-*graft*-hydroxypropyl cellulose (PVP-*g*-HPC) by organocatalyzed visible-light-driven atom transfer radical polymerization (O-ATRP). Employing a "grafting-from" approach, we synthesized a series of PVP-*g*-HPCs with controlled molecular weight and narrow dispersity. By precisely adjusting the molar ratios of HPC and N-vinyl pyrrolidone, we investigated the changes in the lower critical solution temperature (LCST) under various pH conditions. Our results revealed that the thermo-responsive PVP side chains exhibited a reverse dependence on pH. Additionally, the LCST window of HPC thermo-responsive derivatives was expanded to 37 °C within the physiological pH range.

1. Introduction

Over recent decades, stimuli-responsive polymers have become increasingly valuable due to their capacity to respond with precision to environmental changes [1]. These materials can reversibly modify their properties when subjected to external stimuli, including temperature, pH, light, and electrical or magnetic fields [2]. The multifunctional nature and customizable characteristics of these polymers present valuable advantages for various industries, particularly in cosmetics and pharmaceuticals [3]. With a growing emphasis on environmental sustainability and the adoption of vegetarian principles, research has increasingly focused on the development of cellulose-based stimuli-responsive polymers [4].

Hydroxypropyl cellulose (HPC) is a water-soluble, nonionic cellulose ether polymer widely recognized for its utility as an emulsifier in cosmetic formulations and a flocculant in pharmaceuticals due to its neutral charge [5]. Consequently, graft *co*-polymer designs aiming at various applications have been investigated in great detail using HPC as a thermo-responsive backbone. However, the practical application of HPC in various applications is restricted by its lower critical solution temperature (LCST), which lies between 40 and 45 °C. This LCST range can be challenging when aiming for applications close to physiological temperatures, which span from 25 to 38 °C [6]. Although LCST adjustments are achievable through modifications like altering the pH or adding salts [7], another effective approach involves grafting HPC with various monomers. This grafting method makes it possible to adjust the LCST based on the reaction conditions, which makes HPC a desirable thermo-responsive material that can function within the physiological temperature range [8].

Poly(vinylpyrrolidone) (PVP) is another nonionic, thermo-responsive polymer that exhibits a significant response to temperature changes [9]. Additionally, PVP is a biocompatible polymer with unique

* Corresponding authors.
E-mail addresses: toheed@gachon.ac.kr (T. Akhter), chhopark@gachon.ac.kr (C.H. Park).

https://doi.org/10.1016/j.ijbiomac.2025.140856
Received 9 November 2024; Received in revised form 28 January 2025; Accepted 8 February 2025
Available online 12 February 2025
0141-8130/© 2025 Elsevier B.V. All rights are reserved, including those for text and data mining, AI training, and similar technologies.

properties such as strong thermal stability, non-toxicity, antioxidant properties, and solubility in water and various organic solvents [10]. PVP is well-known for its ability to undergo a phase transition, specifically the LCST transition. It is soluble in a given solvent below a certain temperature, but above that temperature, it becomes insoluble and undergoes phase separation [11]. PVP is therefore a viable option for grafting onto HPC in order to control its LCST. Nevertheless, to date, graft copolymers based on HPC and PVP remain largely unexplored, with existing approaches limited to simple physical blends. Such blends often undergo macro-phase separation, restricting each polymer to its inherent properties without intrinsic modulation and hindering the composite's reusability for repeated applications [2].

A cellulose backbone can be grafted with polymers using a variety of techniques [12], including free radical polymerization, reversible deactivation radical polymerization, ring-opening polymerization, nitroxide-mediated polymerization, reversible addition-fragmentation chain transfer polymerization, and atom transfer radical polymerization (ATRP) [13]. One of the most popular controlled radical polymerization techniques for synthesizing cellulose-based graft polymers with specific and distinct architectures is ATRP [14]. Similar to other chemical polymerization techniques, ATRP has certain limitations, primarily concerning potential toxicity. Traditional ATRP methods often employ transition metal catalysts, leading to concerns about metal residues in the resulting polymers [15]. The presence of these metals, even in trace amounts, raises public health concerns due to their potential to interfere with key biological functions in our body [16].

Replacing conventional ATRP with sustainable and environmentally benign variants, such as metal-free organocatalyzed ATRP (O-ATRP), can address these concerns during the preparation of thermo-responsive polymers. In addition to removing concerns about final polymer toxicity, the O-ATRP approach offers an economical way to produce polymers with a low dispersity index (Đ), regulated chain-end functions, and a clearly defined polymer architecture [17]. Additionally, by activating the organic photoredox catalyst with daylight or energy-efficient light-emitting diodes, O-ATRP can also be a green synthetic method [17]. The first effort was reported by Matyjaszewski et al., demonstrating the high effectiveness of phenyl phenothiazine analogs as organic photoredox catalysts in facilitating the O-ATRP of methyl methacrylate (MMA) [18]. Miyake et al. further advanced the field by developing diverse organic photoredox catalysts, including perylene and diaryl dihydrophenazines, for O-ATRP [19]. Similarly, our previous study presented significant progress in O-ATRP by establishing a design principle to develop diverse organic photoredox catalysts [20]. Based on this study, we selected and used 1,2,3,5-tetrakis(carbazol-9-yl)-4,6-dicyanobenzene (4CzIPN) as the organic photoredox catalyst to employ O-ATRP for synthesizing thermo-responsive polymers in our another previous studies [21].

In the current study, we synthesized novel cellulose-based dual-stimuli-responsive PVP-*g*-HPC polymers using the O-ATRP method. Three variants of PVP-*g*-HPC polymers were produced, each with distinct molar ratios of HPC to VP, labeled as HVP-05, HVP-10, and HVP-15. The synthesis began by reacting HPC with 2-bromopropionyl bromide to form a macroinitiator, which was subsequently employed in O-ATRP with vinyl pyrrolidone under visible-light irradiation and 4CzIPN catalysis. To the best of our knowledge, these dual-stimuli-responsive PVP-*g*-HPC polymers have not been previously synthesized via O-ATRP. The LCSTs of the polymers were assessed by monitoring their transmittance changes as a function of temperature. We examined the influence of various pH conditions on the LCST, successfully extending the LCST range of HPC-based thermo-responsive polymers to encompass the physiological temperature range of 25–38 °C. Additionally, we introduced a reverse pH dependency for LCST, increasing the adaptability and controllability of these thermo-responsive polymers. Developing nonionic, cellulose-based thermo-responsive polymers that can be precisely adjusted to suit diverse physiological conditions presents significant potential for a wide range application.

2. Methods

2.1. Materials

Hydroxypropyl cellulose (HPC) was purchased from Carbosynth, UK (Mw = 180,456 $gmol^{-1}$ according to manufacturer), 2-Bromopropionyl bromide (97 %) was purchased from Alfa Aesar. N-Vinyl pyrrolidone (VP, 99.0 %) was purchased from Sigma Aldrish, Dimethyl formamide (DMF, 99.8 %) from RCI Labscan, Thailand, Dichloromethane (DCM, 99 %) were purchased from Sigma Aldrich. 1,2,3,5-tetrakis(ca bazol-9-yl)-4,6-dicyanobenzene (4CzIPN) was prepared using a reported method [22].

2.2. Synthesis of the macroinitiator (HPC-1)

For the synthesis of stimuli-responsive polymers via O-ATRP, a macroinitiator was first prepared using a previously reported procedure [23]. Specifically, 3.6 g of HPC was dissolved in 300 mL of DCM in a round-bottom flask and stirred overnight. The solution was then cooled in an ice bath to 5–10 °C. Next, 279 mg (1.2 mmol) of 2-bromopropionyl bromide, dissolved in 30 mL of DCM, was added dropwise to the solution. The resulting mixture was stirred at room temperature (approximately 30 °C) for 24 h. Subsequently, 30 mL of distilled water was added, causing the formation of a white sticky solid. The mixture was allowed to stand for approximately 30 min to facilitate precipitation. The precipitate was then collected by filtration and vacuum-dried overnight.

Yield, 82 %. Fourier transform infrared (FTIR) (KBr), υ 3462 cm^{-1} (O—H, stretching), 2967, 2911 cm-1 (C—H, stretching), 1728 cm^{-1} (carbonyl group, stretching), 1456 cm^{-1} (CH_2, bending), 1385 cm^{-1} (CH_3, bending). ^1H nuclear magnetic resonance (NMR) ($CDCl_3$), δ 2.04 ppm (br, H of CH_3) 1.27 ppm (br, H of CH_3 from propyloxy groups), 5.2 ppm (br, H of methine).

2.3. Synthesis of poly(N-vinyl pyrrolidone)-g-hydroxypropyl cellulose (PVP-g-HPC)

Three distinct stimuli-responsive polymers HVP-05, HVP-10, and HVP-15 were synthesized using visible-light-driven O-ATRP. The synthesis employed the photoredox catalyst 4CzIPN, as illustrated in Scheme 1(a). The molar ratios of HPC to PVP were varied for each polymer: HVP-05, HVP-10, and HVP-15 had ratios of 95:05, 90:10, and 85:15 (HPC:PVP), respectively. These ratios were determined based on the macroinitiator/monomer feed ratio used in the reaction.

To illustrate, the synthesis of HVP-15 is described in detail. In this process, 337.5 mg of the macroinitiator was dissolved in 3 mL of DMF. Vinyl pyrrolidone (VP, 1.5 mL) and 4CzIPN (15 mg) were then added to the solution. The reaction mixture was purged with nitrogen gas for 30 min. O-ATRP was conducted under blue visible light emitted from a light-emitting diode (LED) setup (20 W, 450 nm) at room temperature for 12 h in a closed system (Fig. S1). After the reaction, the mixture was poured dropwise into methanol while stirring, which resulted in polymer precipitation. The precipitated polymer was collected by filtration and vacuum-dried. In this way, pure PVP-*g*-HPC polymer was obtained using methanol through the co-precipitation method. The yield of the macroinitiator and PVP-*g*-HPC polymer was calculated based on the weight of the purified product relative to the initial weight of hydroxypropyl cellulose used in the synthesis. A 85 % for PVP-*g*-HPC was achieved after purification by precipitation in cold methanol, demonstrating efficient grafting of PVP chains onto the HPC backbone. The thermo-responsive behavior of these polymers was compared with that of pristine HPC.

FTIR (KBr), υ 3442 cm^{-1} (O—H, stretching), 1653 cm^{-1} (amide carbonyl group, stretching), 1731 cm^{-1} (ester carbonyl group, stretching). ^1H NMR (DMSO-d_6), δ 1.2 ppm (br, H of CH_2), 1.8 ppm (br, H of CH_2, PVP ring), 2.1 ppm (br, H of CH_2, PVP ring), 3.3 (br, H of CH_2, PVP

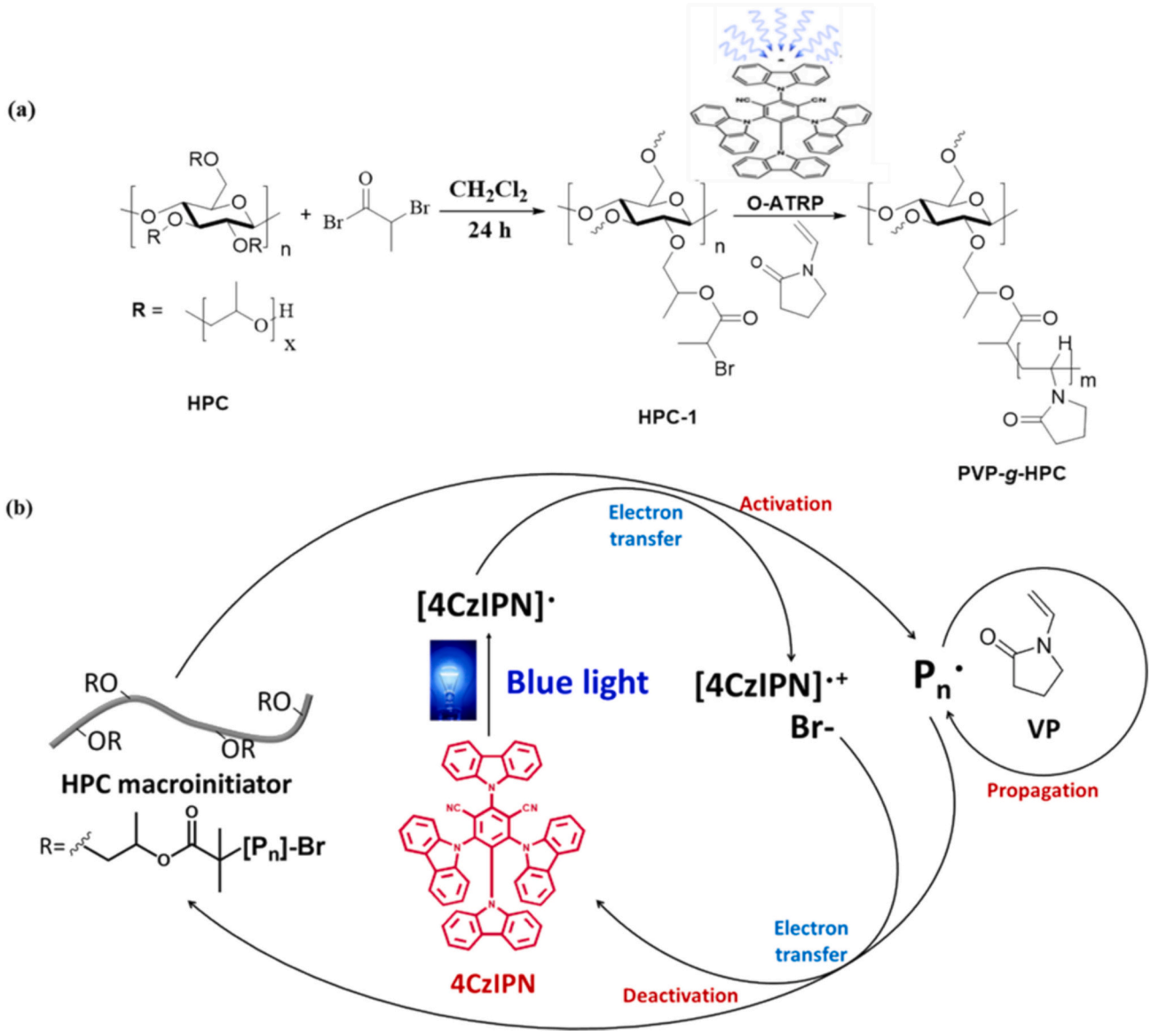

Scheme 1. (a) Synthesis of PVP-*g*-HPC polymers and (b) The O-ATRP mechanism.

ring), 3.6 (br, H of methine).

2.4. Characterizations

The characterization techniques used for the structural analysis of the synthesized polymers are as follows:

2.4.1. Fourier-transform infrared spectroscopy (FTIR)

FTIR spectra of synthesized polymers were recorded using a Shimadzu IRPrestige-21 spectrometer with KBr pellets.

2.4.2. Proton nuclear magnetic resonance spectroscopy (^{1}H NMR)

^{1}H NMR spectra of the synthesized polymers were recorded on a 400 MHz Bruker spectrometer (Germany) using deuterated dimethyl sulfoxide (DMSO-d_6) as the solvent and tetramethyl silane (TMS) as the internal reference. The target HPC used in this study has a molecular substitution (MS) of 2.8 for propylene oxide units, indicating an average of 2.8 propylene oxide units substituted per anhydroglucose unit, as determined by ^{1}H NMR analysis of HPC dissolved in DMSO-d_6.

2.4.3. Gel permeation chromatography (GPC)

To determine the molecular weight and dispersity index (Đ) of the polymers, gel permeation chromatography (GPC) was performed using a Shimadzu 6A system (Japan). The system was calibrated with polystyrene standards for accuracy.

2.4.4. Thermogravimetric analysis (TGA)

TGA was conducted using a TA Instruments Q-50 system to evaluate the thermal properties of the polymers.

2.4.5. The lower critical solution temperature (LCST) determination

The LCST of PVP-*g*-HPC samples was measured using the transmittance method. Transmittance measurements were performed on aqueous solutions (20 mg/mL) at a fixed wavelength of 550 nm using a Shimadzu UV-1800/UV-1900 UV/Visible spectrophotometer, over a temperature range of approximately 20 to 60 °C.

2.4.6. pH effects

The effect of pH on the thermoresponsive behavior of all polymers was assessed by adjusting the pH of the aqueous solutions with NaOH or HCl.

2.4.7. Optical Density (OD) measurement

The OD of polymer solutions at a concentration of 20 mg/mL was measured using a Shimadzu UV-1800/UV-1900 UV/Visible spectrophotometer. Measurements were taken at 570 nm while the temperature was gradually increased from 20 to 60 °C at a heating rate of 10 °C/min.

2.4.8. Hydrodynamic radius (R_h) measurement

Dynamic light scattering (DLS) experiments were performed at a 90° scattering angle using a commercial spectrometer (ALV/SP-150). Before the DLS measurements, polymer solutions were filtered through a Millipore Millex-FH nylon filter (0.40 μm). The hydrodynamic radius (R_h) was calculated by fitting the correlation function using the CONTIN program. Each sample was equilibrated at the specified temperature for 45 min prior to measurement.

3. Results and discussion

3.1. Synthesis and structural analysis of the macroinitiator (HPC-1)

The synthesis of HPC-1 and PVP-*g*-HPC polymers, as well as the O-ATRP mechanism, are illustrated in Scheme 1. Initially, HPC-1 was synthesized by reacting 2-bromopropionyl bromide with HPC. This macroinitiator was then used to graft vinyl pyrrolidone monomers via O-ATRP, resulting in the synthesis of PVP-*g*-HPC stimuli-responsive polymers.

3.2. Synthesis of PVP-g-HPC polymers via O-ATRP

Three distinct stimuli-responsive polymers (HVP-05, HVP-10, and HVP-15) were synthesized using vinyl pyrrolidone and the macroinitiator (HPC-1) through the O-ATRP method. The grafting rates (%) for HVP-05, HVP-10, and HVP-15 were calculated using the equation provided below and were found to be 71 %, 73 %, and 78 %, respectively.

$$\textit{Grafting rate}\ (\%) = \frac{\textit{Weight of PVP} - \textit{g} - \textit{HPC}}{\textit{Initial weight of HPC}} - 1 \times 100 \quad (1)$$

The organic photoredox catalyst 4CzIPN was employed in this process. The synthesis of these stimuli-responsive polymers is illustrated in Scheme 1(a), while Scheme 1(b) depicts the O-ATRP mechanism.

O-ATRP is a versatile and efficient technique that initiates polymerization using visible light in the presence of an organic photoredox catalyst. During this process, the photocatalyst absorbs visible light and utilizes this energy to promote chemical reactions. In this mechanism, 4CzIPN absorbs visible light in its ground state and transitions to an excited state. Through an oxidative process, the photoexcited species can reduce HPC-1, resulting in the production of a bromide anion, a propagating radical (Pn•), and a radical cation.

Subsequently, the controlled propagation of the polymer chains is achieved by sequentially adding monomers. Eventually, deactivation occurs, causing the propagating polymer chains to enter the dormant phase. This process returns the catalyst to its ground state, ultimately completing the O-ATRP cycle. The O-ATRP mechanism has been extensively studied and reported in numerous research publications [20,24].

3.3. FTIR spectroscopy

FTIR spectroscopy was employed to assess the synthesis of the macroinitiator and the structural alterations. The FTIR spectra of HPC and HPC-1 are shown in Fig. 1(a) and (b), respectively. For HPC, the broad absorption band observed at 3455 cm^{-1} was assigned to the stretching vibrations of the HPC hydroxyl group. Additionally, the absorption bands at 2967 cm^{-1} and 2911 cm^{-1} were attributed to the asymmetric and symmetric stretching vibrations of the C—H groups in the CH_3 and CH_2 groups, respectively.

In the case of HPC-1, a new absorption band at 1728 cm^{-1} was

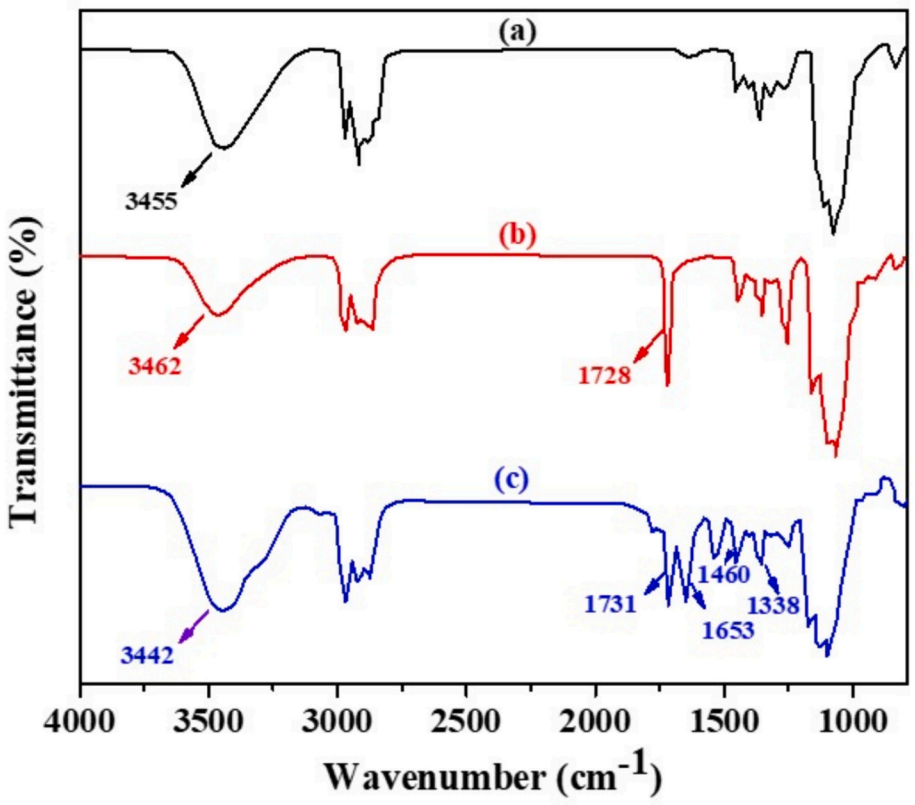

Fig. 1. FTIR spectra of (a) HPC, (b) HPC-1, and (c) PVP-*g*-HPC.

identified as the stretching vibration of the carbonyl group of the ester linkage in the macroinitiator, which was not present in the HPC spectrum. The other absorption bands of HPC-1 matched those of HPC, confirming the structural integrity of the cellulose backbone.

Similarly, the structures of the synthesized polymers were assessed by FTIR spectroscopy. The FTIR spectrum of HVP-15 is shown in Fig. 1 (c). In the FTIR spectrum of HVP-15, both the amide carbonyl group (C=O) of polyvinyl pyrrolidone at 1653 cm^{-1} and the carbonyl group (C=O) of the ester linkage at 1731 cm^{-1} were observed. Notably, the carbonyl peak at 1653 cm^{-1} was absent in the FTIR spectrum of HPC-1, indicating the conversion of HPC-1 into HVP-15. These findings provide strong evidence that PVP chains were successfully grafted onto the HPC surface.

3.4. NMR spectroscopy

The structures of HPC and HPC-1 were evaluated using NMR spectroscopy. Fig. 2 presents the typical ^{1}H NMR spectra of HPC and HPC-1. In the NMR spectrum of HPC-1, a distinct resonance signal at 2.04 ppm (peak (a) in the red line) indicates the presence of methyl groups in the macroinitiator. Another signal at 1.27 ppm (peak (b) in the red line) in the NMR spectrum of HPC-1 can be attributed to the methyl groups on the propyloxy groups. This signal appeared downfield compared to that of HPC, which appeared at 0.8 ppm. The signal at 0.8 ppm was attributed to the methyl group of HPC. Moreover, signal at 4.7 ppm appears on the ^{1}H NMR spectrum, which comes from CH_2- on propoxy group of HPC. The degree of substitution (DS) of 2-Bromopropionyl bromide groups in HPC-1 was determined by comparing the integral area of the proton signal corresponding to the methyl group of the 2-Bromopropionyl bromide group at 2.04 ppm with that of the methyl group in HPC at 0.8 ppm. In this study, macroinitiators HPC-1 with DS_{Br} values of 0.03, 0.06, and 0.12 were employed for the graft copolymerization step in the synthesis of the final polymer. The HPC-1 with a low degree of substitution of the initiating site, DS = 0.03 (one initiating site per tenth glucose units) was used, by which the intermolecular coupling reactions can be minimized between PVP growing side chains during the reaction. Conversely, a macroinitiator with a higher degree of substitution at the initiating site (DS = 0.12) was employed, leading to an increased grafting rate during polymerization. Furthermore, the NMR spectrum of HPC-1 exhibited a resonance signal at 5.2 ppm (peak (c) in the red line) corresponding to methine protons. These results are consistent with previously published literature [25].

NMR spectroscopy was also used to evaluate the structures of the synthesized polymers; Fig. 2 presents the ^{1}H NMR spectrum of HVP-15 as an illustrative example. In this spectrum, the resonance peak at 1.2 ppm (peak (a) in the black line) was assigned to the methylene group of the vinyl component. A methine group was observed at 3.6 ppm (peak (b) in the black line). Additionally, two adjacent methylene groups near the carbonyl group of the pyrrolidone moiety were detected at 1.8 and 2.0 ppm (peaks (c) and (d) in the black line, respectively). Another methylene group located next to the nitrogen atom was observed at 3.3 ppm (peak (e) in the black line). The peaks in the vicinity of $\delta = 1.1$ arise due to overlapping signals from the methyl group protons present in both HPC and PVP. The remaining peaks are attributed to the HPC backbone. These findings are consistent with a previous study [26]. The signals observed at positions (a), (b), (c), (d), and (e) in the NMR spectrum of HVP-15 correspond to the protons of the PVP side chains. Therefore, the NMR data further confirmed that the PVP chains were successfully grafted onto the HPC surface.

3.5. GPC Analysis of HPC and PVP-g-HPC

The M_n and Đ of HPC, HVP-05, HVP-10, and HVP-15 polymers were determined through gel permeation chromatography (GPC) analysis. Fig. 3 shows the chromatograms of all the polymers, and Table 1 presents their M_n and Đ values. The data indicate that all of the synthesized polymers possess a narrow Đ, with values of 1.2, 1.2, and 1.1 for HVP-05, HVP-10, and HVP-15, respectively, even at high M_n values.

In conclusion, the O-ATRP technique appears to be highly effective for producing monodisperse polymers with narrow Đ values and is free from metal contamination. Furthermore, the hydrodynamic volumes (V_h) of HPC, HVP-05, HVP-10, and HVP-15 were determined by applying the Mark–Houwink equation, and the results are shown in Table 1 [27]. The results obtained from the GPC analysis indicate that the PVP-*g*-HPC polymers have higher V_h values than HPC. Additionally, the V_h of PVP-*g*-HPC increased as the M_n of the polymer increased.

3.6. Polymerization kinetics

The GPC analysis was utilized to study the polymerization kinetics, with HVP-15 being used for conducting the kinetic investigations. Fig. 4 illustrates the conversion of the monomer versus time, which is

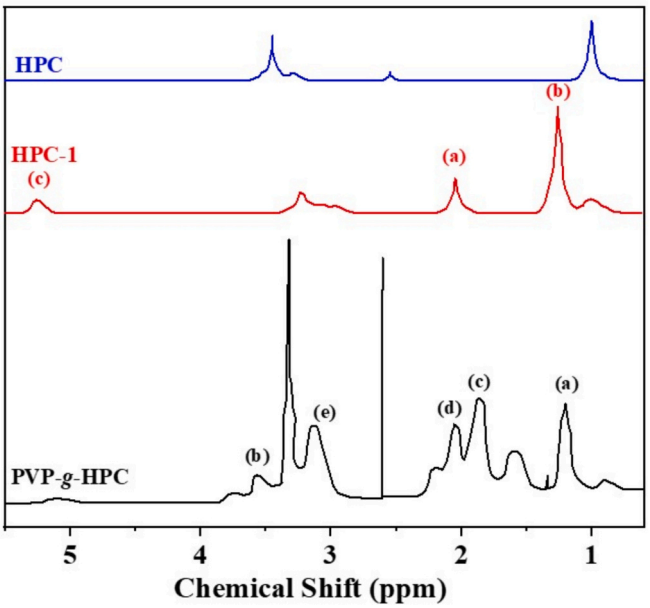

Fig. 2. ^{1}H NMR spectra of HPC, HPC-1, and PVP-*g*-HPC.

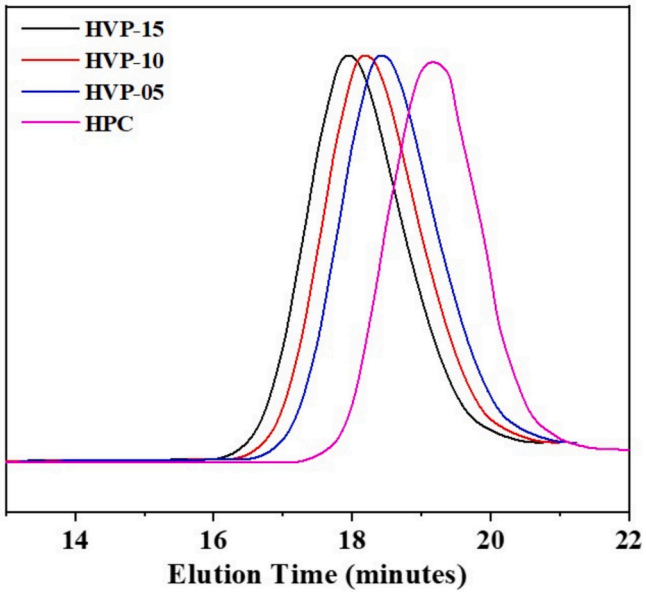

Fig. 3. GPC chromatograms of HPC, HVP-05, HVP-10, and HVP-15 polymers.

Table 1
Molecular weight, dispersity index, and hydrodynamic volume of HPC, HVP-05, HVP-10, and HVP-15 polymers.

Sample	M_n (g mol^{-1})	(Đ)	V_h (mL mol^{-1})
HPC	180,456	1.8	1.61×10^6
HVP-05	253,036	1.2	2.26×10^6
HVP-10	278,394	1.2	2.49×10^6
HVP-15	303,475	1.1	2.87×10^6

M_n = number-average molecular weight. V_h = hydrodynamic volume. Đ = dispersity index. Reaction conditions: Synthesis of polymers was carried out in an inert atmosphere of nitrogen at 2 5 °C under the irradiation of 20 W, 450 nm blue LEDs (5 mW cm^{-2}).

represented using a semi-logarithmic plot. The initial concentration of the monomer is denoted as M_o, whereas the concentration of the monomer at a specific time is denoted as M_t. In Fig. 4(a), a linear relationship is observed for the plot of $\ln([M]_o/[M]_t)$ versus time, specifically from the start of polymerization until approximately 3 h. This linear trend suggests that first-order kinetics occurred during this period [28]. After the initial linear phase, the graph in Fig. 4(a) displays a slight curvature, indicating a deviation from the previously observed linear behavior. This deviation can be attributed to factors such as the use of a polar solvent (DMF) or a reduction in the radical concentration, which could result in the partial termination of living free radicals. Furthermore, the apparent propagation rate constant (k_{app}) was calculated as 0.03 h^{-1} using Eq. (2) [30].

$$ln\left(\frac{[M]_o}{[M]_t} = k_{app} \times t\right) \quad (2)$$

Fig. 4(b) exhibits the variation in the Đ and M_n of PVP side chains versus the monomer conversion, and these PVP chains were obtained by hydrolyzing PVP-*g*-HPC. Fig. 4(b) demonstrates a slight variation in both the M_n and Đ of the PVP side chains, providing additional evidence for the observed polymerization kinetics. GPC traces of the PVP side chains at different time intervals are presented in Fig. 4(c). Additionally, the data displays that as the monomer conversion increased, the M_n of PVP increased with controlled Đ during the polymerization process. These findings suggest that O-ATRP is a highly controlled process, and the results obtained are consistent with those of previous research studies [31].

3.7. TGA analysis of HPC and PVP-g-HPC

The thermal properties of HPC, HPC-1, HVP-05, HVP-10, and HVP-15 were characterized by thermogravimetric analysis (TGA). The thermograms of these materials are presented in Fig. S2, and their thermal stabilities were examined in terms of T_5, T_{10}, T_{50}, and R_{600}, as shown in Table S1. The thermogram shows that HPC undergoes a single-step degradation process with a T_{50} value of 374 °C. Compared with that of HPC, the thermal stability of HPC-1 was significantly reduced (T_{50} = 251 °C), although decomposition still occurred in a single step. The decreased thermal stability of HPC-1 can be correlated to the presence of bromoalkyl groups, which undergo the elimination of hydrogen bromide when exposed to heating conditions during TGA analysis [32]. For PVP-*g*-HPC polymers, the thermal degradation occurs in two distinct stages. The initial weight loss observed at approximately 100 °C might have originated from the elimination of any trapped moisture. The first stage of degradation takes place within the temperature range of 240 to 338 °C, while the second stage begins at approximately 375 °C and continues until 490 °C. HVP-15 demonstrated a T_{50} value of 388 °C, which was higher than those of HPC and HPC-1. This improved thermal stability may be primarily attributed to the chain extension that occurred during the synthesis of the final polymer [33]. HVP-15 also exhibited a lower R_{600} value than those of HPC and HPC-1. As shown in Fig. S2, the thermal stabilities of HVP-05 and HVP-10 exhibited similar

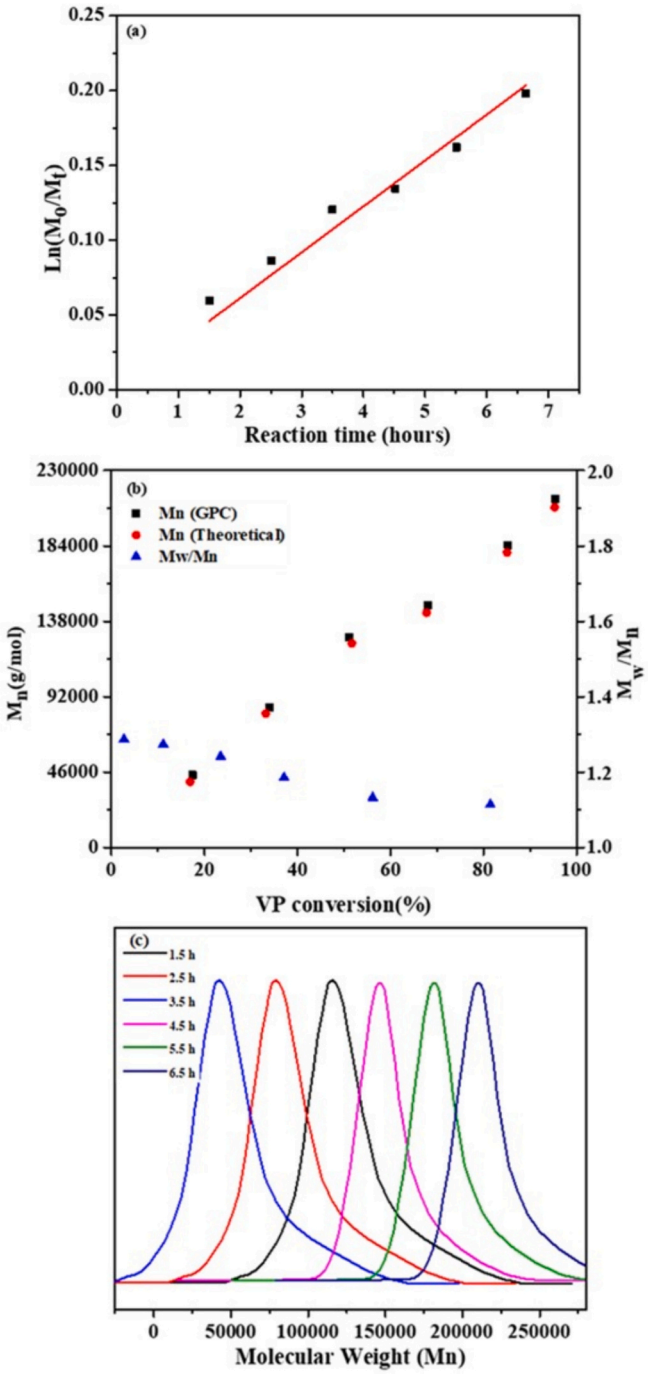

Fig. 4. (a) Relationship between monomer consumption and the reaction time. (b) Variation in Đ and M_n of PVP side chains with respect to the monomer conversion. (c) GPC Traces of PVP side chains extracted from the reaction mixture at different time intervals.

trends. These findings indicate significant differences in the thermal stabilities of HPC and HPC-1, providing evidence for the successful synthesis of these polymers.

3.8. Dual-responsive behavior of PVP-g-HPC polymers

The pH- and thermo-responsive behaviors of the HPC, HVP-05, HVP-10, and HVP-15 in aqueous solution were investigated by exploring their LCSTs, as illustrated in Fig. 5. The LCSTs were determined by analyzing the transmittance profile. The LCST of HPC was observed to be 43.6 °C in pH 3.2, with a gradual increase in LCST as the pH increased, reaching

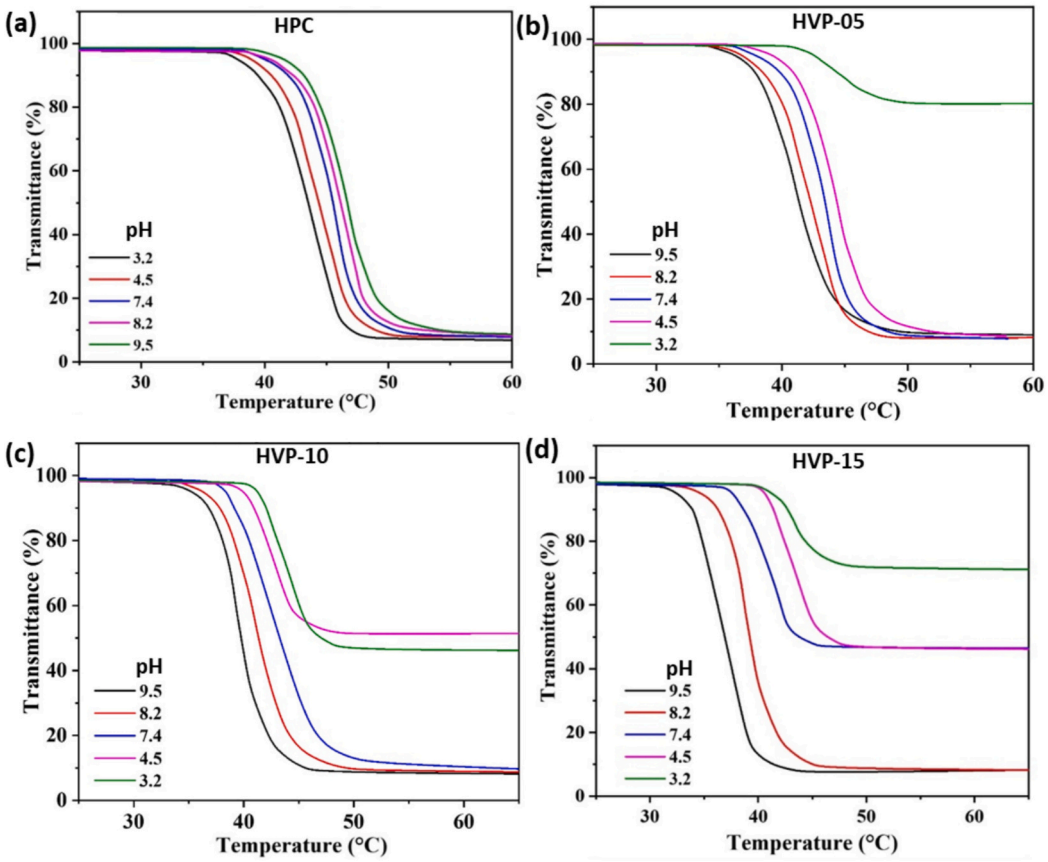

Fig. 5. The transmittance of (a) HPC, (b) HVP-05, (c) HVP-10, and (d) HVP-15 vs. temperature as a function of pH.

46.6 °C in pH 9.5 (Fig. 5(a)). In contrast, the results demonstrated that increasing the pH resulted in a decrease in the LCST of the polymers, as observed in the case of HVP-05, HVP-10, and HVP-15 (Fig. 5b–d). The LCSTs were observed to be 43.4–43.8 °C in pH 3.2 solution of HVP-05, HVP-10, and HVP-15. Upon changing the pH to a more basic level, the LCSTs were found to decrease to 41.3, 39.4, and 37.2 °C for HVP-05, HVP-10, and HVP-15, respectively. In particular, PVP-*g*-HPC exhibited the high equilibrium transmittance values at temperatures above the LCST in acidic conditions. This trend was most pronounced with the long PVP side chains. For instance, the transmittance of HVP-15 decreased to approximately 70 % and 45 % at low pH values of 3.2 and 4.5, respectively. The high transmittance above LCST indicates a less aggregated state of polymer in equilibrium, and partial self-assembled polymer chains can be ascribed to these phenomena [33]. PVP chains are known to undergo protonation in an acidic solution, which can increase the electrostatic repulsion and ultimately hinder phase separation [34]. These findings are in good agreement with those of previous studies [35].

Fig. 6(a) depicts the summarized pH dependency of the LCST of polymers. An increase in pH resulted in an increase in the LCST value of HPC, whereas the LCST decreased with increasing pH for HVP-05, HVP-10, and HVP-15. Fig. 6(b) describes the differences in the LCST behavior between HPC and the PVP-*g*-HPC series with respect to changes in pH. In the case of HPC, the formation of hydrophobic aggregates caused by the cleavage of hydrogen bonds between HPC and water molecules [36]. The LCST of HPC was lower in an acidic solution and higher in a basic solution than in neutral pH, because the polymer chains become relatively hydrophilic as hydroxy groups are ionized to O^- in basic condition. Compared to the HPC, the presence of solvent molecules allows hydration and interaction with the PVP-*g*-HPC at a temperature lower than the LCST, resulting in a homogeneous solution. As the temperature rose above the LCST, the interactions between the polymer and the solvent began to weaken, leading to a shift in the equilibrium between the polymer–solvent and polymer–polymer interactions. Consequently, the weakening of the polymer–solvent interactions resulted in the aggregation or phase separation of PVP-*g*-HPC [37]. The lower LCST of PVP-*g*-HPC compared to that of HPC can be attributed to the formation of hydrogen bonds between the hydrogen bond donor (HPC) and the hydrogen bond acceptor (ester groups of PVP) [38]. Also, the LCST of PVP-*g*-HPC was lower in the basic solution than in the acidic solution. Meaning, that the PVP-*g*-HPC is more soluble in acid medium compared to the base medium since the grafted PVP chains are protonated and generate electrostatic repulsion. As evidence, PVP-*g*-HPCs at the temperatures above LCST under acidic conditions is more transparent than that of pristine HPC. Especially, this trend is clear in the HVP-15, which has a relatively long PVP, as shown in Fig. 5(d).

3.9. Optical measurement in response to temperature and pH

3.9.1. Hydrodynamic radius

Fig. 7 illustrates the changes in hydrodynamic radius (R_h) of HVP-15 across different temperatures and pH values. To determine the R_h, we used an aqueous polymer solution at a concentration of 1 mg/mL. As shown in Fig. 7, at a pH of 4.5, the R_h remained relatively constant as the temperature was raised from 25 °C to 43 °C, after which a gradual increase in R_h was observed. A similar trend was noted at pH values of 7.4, 8.2, and 9.5, where R_h initially remained stable before sharply increasing at temperatures of 42 °C, 39 °C, and 37 °C, respectively. Notably, the behavior of both R_h and LCST in response to temperature and pH variations suggests a close correlation between these properties.

3.9.2. Optical density

Fig. 8 illustrates the optical densities for the HPC, HVP-05, HVP-10, and HVP-15 polymers, measured at 550 nm as their aqueous solutions

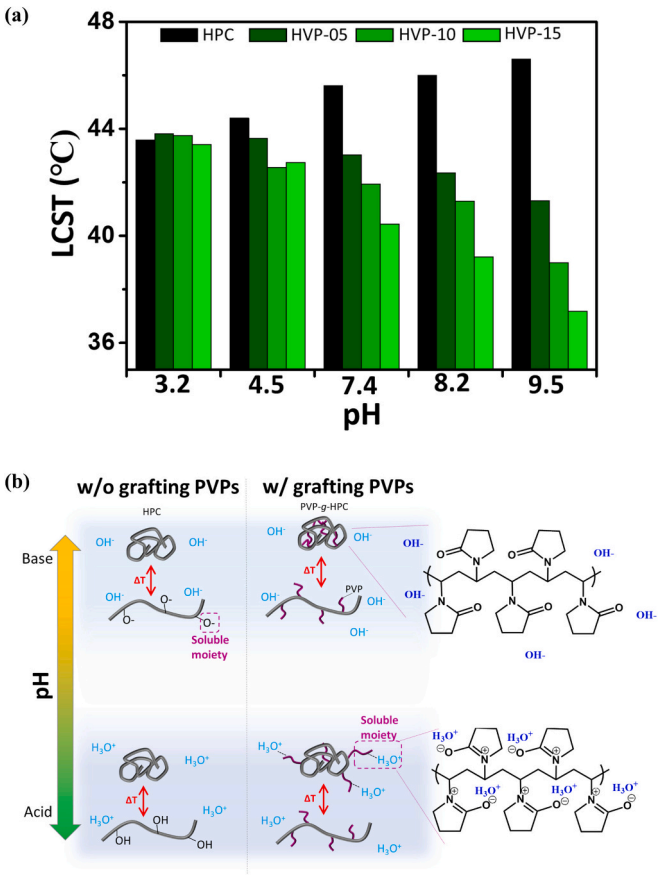

Fig. 6. (a) The LCST of HPC, HVP-05, HVP-10, and HVP-15 as a function of the pH value. (b) Mechanism of the thermo-responsive behavior of the HPC and PVP-*g*-HPC depending on pH condition.

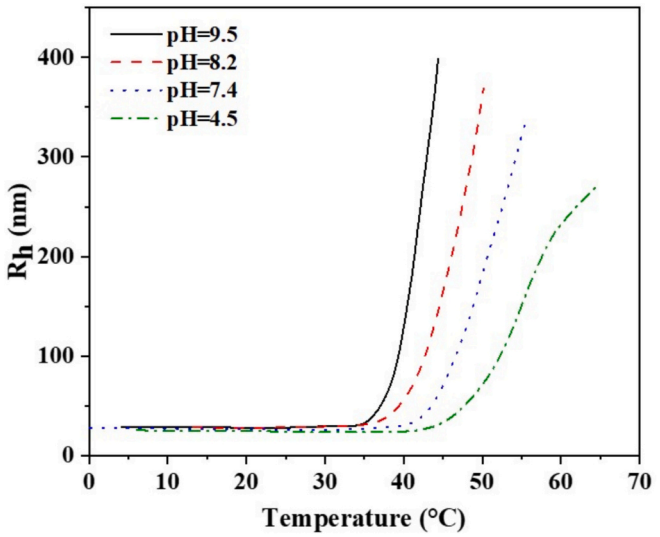

Fig. 7. Temperature dependence of the hydrodynamic radius (R_h) of HVP-15 in an aqueous solution at different pH values.

were gradually heated from 25 to 65 °C. Within the 25 to 43.5 °C range, HPC maintained a low optical density of approximately 0.198, signifying its high solubility in water under these conditions. This behavior arises from HPC's LCST characteristics in water. Below its LCST, HPC remains highly soluble, forming a uniform aqueous solution [21]. As the temperature rose from 43.5 to 65 °C, HPC lost its solubility, causing its

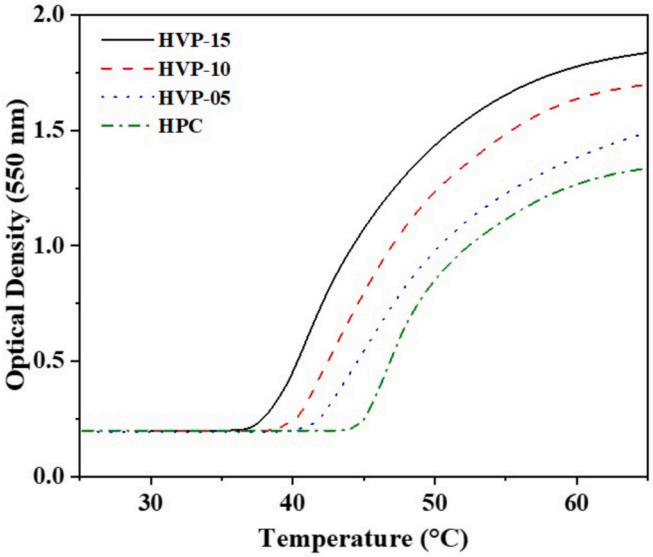

Fig. 8. Optical density of HPC, HVP-05, HVP-10, and HVP-15 polymers in an aqueous solution.

optical density to rise significantly, reaching a value of 1.32. Once the temperature exceeds the LCST of HPC, the polymer chains experience a phase shift, resulting in the formation of a distinct phase that often appears cloudy or gel-like within the solution. This separation occurs because, above the LCST, the interactions between the polymer and water molecules change significantly, prompting the HPC molecules to cluster together rather than remain evenly dispersed in the water [21,39].

For HVP-15, the optical density stayed steady at approximately 0.2 up to 37 °C, after which it rose significantly, reaching 1.83 at 65 °C. This transition indicates that heating beyond 37 °C induces the polymer to begin aggregating. This aggregation behavior can be ascribed to the PVP segments in the polymer, which act as hydrophobic regions in water, prompting the formation of clusters. Similarly, HVP-05 and HVP-10 maintained their initial optical density values up to approximately 42 °C and 39 °C, respectively. Beyond these temperatures, their optical densities increased with rising temperature, reaching maximum values of 150 and 170 at 65 °C.

The rise in optical density observed at higher temperatures can be attributed to the dehydration of HPC components, which intensifies the hydrophobic interactions among the PVP segments. As the temperature escalates, water molecules associated with the hydrophilic groups in HPC are released, leading to decreased solubility. This dehydration exposes the hydrophobic core of the HPC segments, prompting the aggregation of polymer chains. In addition, PVP experiences LCST transition; when the temperature surpasses this threshold, the PVP segments transition to a hydrophobic state, resulting in phase separation and further aggregation. This enhanced aggregation boosts the hydrophobic interactions between the polymer chains, which contributes to the observed increase in optical density. These findings are consistent with previous research [40].

Table 2 displays a comparison of type of polymer, molecular weight, polydispersity, and LCST for understanding differences in the HPC or PVP-based thermo-responsive polymers between the current research and earlier studies. Regarding bio application, the temperature operating range guaranteed to be safe in the body is less than 45 °C [2]. The conventional temperature-relevant treatment, including hyperthermia treatment and photothermal therapy, are only considered in a particular range since cell necrosis and death are enacted within several minutes at above 48 °C regardless of the lesion or not [41]. In this regard, LCSTs of our polymer system well corresponds to the temperature range from body temperature to conventional thermal therapy range.

Table 2
Comparison of type, molecular weight, polydispersity, and LCST of HPC or PVP-based polymers.

#	Polymer	Mn (g mol-1)	Đ	LCST (°C)	Ref.
1	HPC-*g*-PDEGMA	30,400-32,780	1.5–1.2	27–22	[42]
2	HPC-*g*-P(OEGMA-co-DEGMA)	21,200-58,100	1.6–1.1	59–33	[43]
3	HPC-*g*-P(NIPAAm)	40,600-71,800	1.8–1.9	34.7–33.3	[44]
4	EPVP-*b*-PVP	4900-25,500	1.6–1.3	38.5–30.1	[45]
5	PMVC-PVP	8900-10,100	1.7–1.2	19.2–15.2	[46]
6	P(MVC-co-VC)-*b*-PVP	32,400	1.7–1.4	28–46	[47]
7	PCL-*b*-(PVCL-co-PVP)	13,200-16,500	1.08–1.04	30.1–40.4	[48]
8	PVP-*co*-P(TEGMA)	14,400-26,780	1.6–1.3	36–61	[49]
9	PMMA-*g*-HPC	180,456-291,075	1.8–1.1	36.7–44.3	[21]
10	PVP-*g*-HPC	180,456-303,475	1.8–1.1	37–43	This work

4. Conclusion

In conclusion, this work synthesized dual, temperature- and pH-, responsive PVP-*g*-HPC polymer brushes using a visible-light-driven O-ATRP method. By adjusting the molar ratio of the PVP grafting polymer chain, the LCST of the PVP-*g*-HPC polymers was controlled to be close to the human body temperature (25–40 °C). The "grafting-from" approach using O-ATRP allowed us to achieve a high degree of control and fidelity in the polymerization process, leading to well-defined molecular structures and very low Đ values of 1.1 for these high M_n polymers. The pH dependence and LCST trend of the PVP-*g*-HPC polymers were influenced by the M_n of the grafted PVP segments. For the HVP-15 polymer with the highest M_n, the LCST of PVP-*g*-HPC decreased from 43 to 37 °C as the pH increased from 3.2 to 9.5, compared to the pristine HPC which has the LCST from 43.5 to 46 °C as the pH value increased from 3.2 to 9.5. Overall, these findings offer insights into the design of advanced cellulose derivatives with tailored phase behaviors, broadening their applicability in biocompatible and environmentally adaptive materials. By expanding the pH-dependent LCST range and achieving reversible responsiveness, this work provides a foundation for developing novel stimuli-responsive systems for biomedical, pharmaceutical, and environmental applications, aligning with the interdisciplinary and translational research objectives.

CRediT authorship contribution statement

Muhammad Asif Iqbal: Writing – original draft, Methodology, Formal analysis, Conceptualization. **Sadaf Ul Hassan:** Validation. **Asif Mahmood:** Resources. **Waheed Al-Masry:** Resources. **Junhyuk Lee:** Writing – review & editing. **Hyun Jong Lee:** Writing – review & editing. **Toheed Akhter:** Writing – review & editing, Writing – original draft, Validation, Supervision, Conceptualization. **Chan Ho Park:** Writing – review & editing, Resources.

Declaration of Generative AI and AI-assisted technologies in the writing process

During the preparation of this work the authors used ChatGPT in order to improve the language. After using this tool, the authors reviewed and edited the content as needed and take full responsibility for the content of the publication.

Declaration of competing interest

The authors declare that they have no known competing financial interests or personal relationships that could have appeared to influence the work reported in this paper.

Acknowledgement

This work was supported by the National Research Foundation of Korea (NRF) grant funded by the Korean government (MSIT) (RS-2023-00251670; RS-2024-00408370).

Appendix A. Supplementary data

Supplementary data to this article can be found online at https://doi.org/10.1016/j.ijbiomac.2025.140856.

Data availability

No data was used for the research described in the article.

References

[1] a S.J. Lugger, S.J. Houben, Y. Foelen, M.G. Debije, A.P. Schenning, D.J. Mulder, Chem. Rev. 122 (2021) 4946–4975;
b C.H. Park, I.A. Thompson, S.S. Newman, L.A. Hein, X. Lian, K.X. Fu, J. Pan, M. Eisenstein, H.T. Soh, Adv. Mater. 36 (2024) 2306704;
c S.J. Lugger, S.J. Houben, Y. Foelen, M.G. Debije, A.P. Schenning, D.J. Mulder, Chem. Rev. 122 (2021) 4946–4975.
[2] a C.H. Park, T. Kim, G.H. Lee, K.H. Ku, S.H. Kim, B.J. Kim, Acs Appl. Mater. Inter. 12 (2020) 35415–35423;
b X.Z. Yan, F. Wang, B. Zheng, F.H. Huang, Chem. Soc. Rev. 41 (2012) 6042–6065;
c G. Jeong, T. Kim, S.D. Park, M.J. Yoo, C.H. Park, H. Yang, Macromol. Rapid Commun. 45 (2024) e2300542.
[3] a J.M. Korde, B. Kandasubramanian, E.C. Research, Ind. Eng. Chem. Res. 58 (2019) 9709–9757;
b C.H. Park, H. Yun, H. Yang, J. Lee, B.J. Kim, Adv. Funct. Mater. 27 (2017) 1604403.
[4] a H. Ullah, H.A. Santos, T. Khan, Cellulose 23 (2016) 2291–2314;
b X. Yan, F. Wang, B. Zheng, F. Huang, Chem. Soc. Rev. 41 (2012) 6042–6065.
[5] a H.C. Arca, L.I. Mosquera-Giraldo, V. Bi, D.Q. Xu, L.S. Taylor, K.J. Edgar, Biomacromolecules 19 (2018) 2351–2376;
b K.A. Heitfeld, T. Guo, G. Yang, D.W. Schaefer, Mat Sci Eng C-Bio S 28 (2008) 374–379;
c M. Gosecki, H. Setala, T. Virtanen, A.J. Ryan, Carbohydr. Polym. 251 (2021) 117015;
d H. Ullah, H.A. Santos, T. Khan, Cellulose 23 (2016) 2291–2314.
[6] a M. Gosecki, H. Setälä, T. Virtanen, A.J.J.C.P. Ryan, Carbohydr. Polym. 251 (2021) 117015;
b S. Graham, P.F. Marina, A. Blencowe, Carbohydr. Polym. 207 (2019) 143–159.
[7] a P. Khuman, W.B.K. Singh, S.D. Devi, H. Naorem, Part A, J. Macromol. Sci. 51 (2014) 924–930;
b X. Xia, S. Tang, X. Lu, Z. Hu, Macromolecules 36 (2003) 3695–3698.
[8] H. Kang, R. Liu, Y.J.P. Huang, Polym. Chem. 70 (2015) A1–A16.
[9] a C. Jiao, Y. Chen, T. Liu, X. Peng, Y. Zhao, J. Zhang, Y. Wu, H. Wang, Interfaces 10 (2018) 32707–32716.
[10] a L.K. Mireles, M.-R. Wu, N. Saadeh, L.H. Yahia, E. Sacher, ACS Omega 5 (2020) 30461–30467;
b B. Singh, A. Kumar, Food Hydrocoll. Health 1 (2021) 100008;
c K. Ramesh, R.K. Gundampati, S. Singh, K. Mitra, A. Shukla, M.V. Jagannadham, D. Chattopadhyay, N. Misra, B. Ray, RSC Adv. 6 (2016) 25864–25876.
[11] Q. Feng, Y. Zhao, H. Li, Y. Zhang, X. Xia, Q.J.C. Yan, P. Sci. 296 (2018) 165–172.
[12] S. Wohlhauser, G. Delepierre, M. Labet, G. l. Morandi, W. Thielemans, C. Weder, J. o. Zoppe, Macromolecules 2018, 51, 6157–6189.
[13] aK. Parkatzidis, H. S. Wang, N. P. Truong, A. Anastasaki, Chem, Volume 6, Issue 7, 1575 - 1588.
bM. Chen, M. Zhong, J. A. Johnson Chem. Rev. 2016, 116, 17, 10167–10211.
cC.-W. Tu, F.-C. Tsai, C.-J. Chang, C.-H. Yang, S.-W. Kuo, J. Zhang, T. Chen, C.-F. Huang, Polymers 11 (2019) 1631.
[14] aF. Lorandi, M. Fantin, K. Matyjaszewski, J. Am. Chem. Soc. 2022, 144, 15413–15430.
bM. Kumar, P. S. Gehlot, D. Parihar, P. K. Surolia, G. Prasad, Eur. Polym. J. 2021, 152, 110448.
[15] aF. Perin, A. Motta, D. Maniglio, 2021, Mater. Sci. Eng. C 123, 111952. b A. Najer, D. Wu, D. Vasquez, C.G. Palivan, W. Meier, Nanomedicine 8 (2013) 425–447.
[16] aD. J. Siegwart, J. K. Oh, K. Matyjaszewski, Prog. Polym. Sci. 2012, 37, 18–37.
bG. Szczepaniak, J. Piątkowsk, W. Nogaś, F. Lorandi, S.S. Yerneni, M. Fantin, A. Ruszczyńska, A.E.Enciso, E. Bulska, K. Grela, K. Matyjaszewski. Chem. Sci., 2020, 11, 4251-4262.
cP. R. Rodrigues, R. Vieira, Eur. Polym. J. 2019, 115, 45–58.
[17] D. A. Corbin, G.M. Miyake, Chem. Rev. 2021, 122, 1830–1874.

[18] J. C. Theriot, C.-H. Lim, H. Yang, M. D. Ryan, C. B. Musgrave, G.M. Miyake, 2016, Science 352, 1082–1086.
[19] J. C. Theriot, B. G. McCarthy, C. H. Lim, G.M. Miyake, Macromol. Rapid Commun. 2017, 38, 1700040.
[20] V.K. Singh, C. Yu, S. Badgujar, Y. Kim, Y. Kwon, D. Kim, J. Lee, T. Akhter, G. Thangavel, L.S. Park, J. Lee, P.C. Nandajan, R. Wannemacher, B. Milián-Medina, L. Lüer, K.S. Kim, J. Gierschner, M.S. Kwon, Nat. Catal. 2018, 1, 794–804.
[21] aM. A. Iqbal, T. Akhter, M. Faheem, A. Mahmood, W. Al-Masry, S. Nadeem, S. Ul Hassan, C. H. Park, Cellulose 2023, 30, 7519-7533. b M.A. Iqbal, A. Mahmood, W. Al-Masry, C.H. Park, S.U. Hassan, T. Akhter, Polym. Chem. (15) (2024) 4244–4254.
[22] M.A. Iqbal, A. Mahmood, W. Al-Masry, C.H. Park, S.U. Hassan, T. Akhter, Polym. Chem. 15 (2024) 4244–4254.
[23] K. Rahimian, Y. Wen, J.K. Oh, Polymer 2015, 72, 387–394.
[24] X. Pan, C. Fang, M. Fantin, N. Malhotra, W.Y. So, L.A. Peteanu, A.A. Isse, A. Gennaro, P. Liu, K. Matyjaszewski, J. Am. Chem. Soc. 138 (2016) 2411–2425.
[25] M. Bagheri, L. Pourmirzaei, Macromol. Res. 2013, 21, 801–808.
[26] T. Wang, L. Jin, Y. Zhang, Y. Song, J. Li, Y. Gao, S. Shi, Polym. Bull. 75 (2018) 4485–4498.
[27] a M.R. Kasaai, Carbohydr. Res. 343 (2008) 2266–2277;
b A. Mehta, J. Pandey, G.J.M.S. Sen, E. B, Mater. Sci. 263 (2021) 114750.
[28] aM. Yang, S. Xie, Q. Li, Y. Wang, X. Chang, L. Shan, L. Sun, X. Huang, C. Gao, Int. J. Pharm. 2014, 465, 187–196.
bE. Bulut, Y. Turhan, Int. J. Biol. Macromol. 2021, 191, 1191–1203.
[30] R.R. Palem, S.D. Ganesh, N. Saha, J. Kronek, P. Sáha, J. Polym. Res. 25 (2018) 1–12.
[31] a M. Doreth, K. Löbmann, P. Priemel, H. Grohganz, R. Taylor, R. Holm, H.L. de Diego, T. Rades, Biopharm. Europ. J. Pharm. 122 (2018) 62–69;
b M. Tarnacka, P. Maksym, A. Zięba, A. Mielańczyk, M. Geppert-Rybczyńska, L. Leon-Boigues, C. Mijangos, K. Kamiński, M. Paluch, Chem. Commun. 55 (2019) 6441–6444.
[32] E. Oestmark, S. Harrisson, K.L. Wooley, E.E. Malmström, Biomacromolecules 8 (2007) 1138–1148.
[33] C.H. Park, S. Lee, G. Pornnoppadol, Y.S. Nam, S.-H. Kim, B.J. Kim, ACS Appl. Mater. Interfaces 10 (2018) 9023–9031.
[34] a M. Loría-Bastarrachea, W. Herrera-Kao, J. Cauich-Rodríguez, J. Cervantes-Uc, H. Vázquez-Torres, A. Ávila-Ortega, Calorimetry 104 (2011) 737–742;
b L. Wang, R. Zeng, C. Li, R. Qiao, Colloids Surf. B: Biointerfaces 74 (2009) 284–292.
[35] a S. Jin, M. Liu, S. Chen, C. Gao, European Polym. J. *44* (**2008**) 2162–2170;
b M. Sponchioni, U.C. Palmiero, D. Moscatelli, E. C, Mater. Sci. 102 (2019) 589–605;
c M. Gosecki, H. Setälä, T. Virtanen, A.J. Ryan, Carbohydr. Polym. 251 (2021) 117015.
[36] aY. Bai, W. Chen, T. Tang, Y. He, Solar Energy 2022, 245, 376–384.
bT. M. S. U. Gunathilake, Y. C. Ching, C. H. Chuah, N. Abd Rahman, N.S. Liou, Int. J. Biol. Macromol. 2020, 158, 670–688.
[37] aP. Shao, B. Wang, Y. Wang, J. Li, Y. Zhang, J. Nanomater. 2011, 2011, 1–12.
b F. Qian, J. Wang, R. Hartley, J. Tao, R. Haddadin, N. Mathias, M. Hussain, Pharm. Res. 29 (2012) 2766–2776.
[38] Y. Zhang, X. Du, H. Wang, Z. He, H. Liu, 2021, 18, 515–526.
[39] C.H. Park, H. Yang, J. Lee, H.-H. Cho, D. Kim, D.C. Lee, B.J. Kim, Chem. Mater. 27 (2015) 5288–5294.
[40] a Y.S. Yang, Y. Zhou, F.B.Y. Chiang, Y. Long, RSC Advances 6 (2016) 61449–61453;
a E. Weißenborn, B. Braunschweig, Soft Matter 15 (2019) 2876–2883.
[41] X.J. Zhu, W. Feng, J. Chang, Y.W. Tan, J.C. Li, M. Chen, Y. Sun, F.Y. Li, Nat. Commun. 7 (2016) 10437.
[42] C. Porsch, S. Hansson, N. Nordgren, E. Malmström, Polym. Chem. 2 (2011) 1114–1123.
[43] a J.-F. Lutz, K. Weichenhan, Ö. Akdemir, A. Hoth, Macromolecules 40 (2007) 2503–2508;
b C. Porsch, S. Hansson, N. Nordgren, E. Malmström, Polym. Chem. (2) (2011) 1114–1123.
[44] F. Xu, Y. Zhu, F. Liu, J. Nie, J. Ma, W.T. Yang, Bioconjug. Chem. 21 (2010) 456–464.
[45] J. Giliomee, R. Pfukwa, N.P. Gule, B. Klumperman, Polym. Chem. 7 (2016) 1138–1146.
[46] V. Kozlovskaya, F. Liu, Y. Yang, K. Ingle, S. Qian, G. V. Halade, V. S. Urban, E. Kharlampieva, Biomacromolecules 2019, 20, 3989–4000.
[47] X. Liang, F. Liu, V. Kozlovskaya, Z. Palchak, E. Kharlampieva, ACS Macro Lett. 4 (2015) 308–311.
[48] Y.C. Yu, G. Li, J. Kim, J.H. Youk, Polymer 54 (2013) 6119–6124.
[49] C. Jumeaux, R. Chapman, R. Chandrawati, M.M. Stevens, Polym. Chem. 6 (2015) 4116–4122.